Bruno BAPTISTA[1], André MENDES[1], Sérgio CRUZ[1], António CARDOSO[1]

University of Coimbra / Instituto de Telecomunicações (1)

Temperature Distribution Inside a Three-Phase Induction Motor Running with Eccentric Airgap

Abstract. *Despite the emergence of new types of electric machines, the squirrel-cage induction motor remains the dominant one. A motor failure can result in large lost revenues. One of types of faults that can occur in these motors is airgap eccentricity. This paper presents results, based on a Finite Element Analysis. It is shown that static eccentricity leads to a non-uniform temperature distribution and contributes to the rise of the highest temperature spot in the motor, hence potentially shortening the lifespan of the stator insulation system.*

Streszczenie. *Klatkowy silnik indukcyjny wciąż dominuje wśród maszyn elektrycznych. Jednym z typowych uszkodzeń tego silnika jest ekscentrycvz ność szczeliny powietrznej. Przeprowadzono analizę tego zjawiska wykorzystując metodę elementu skończonego. Statyczna ekscentryczność powoduje nierównomierny rozkład temperatury. (**Rozkład temperatury w trzyfazowym silniku indukcyjnym z ekscentryczną szczeliną powietrzną**)*

Keywords: Airgap eccentricity, Induction Motor, Temperature, UMP.
Słowa kluczowe: silnik indukcyjny, rozkład temperatury, ekscentryczność.

Introduction

Airgap eccentricity is a fault mechanism which can occur in induction motors where the airgap between the stator and rotor is no longer uniform. The reasons for eccentricity include intrinsic shaft tolerance, ball-bearings defects or problems related with the fixing of these motor parts [1, 2].

Eccentricity is usually classified as static, dynamic and mixed. Static eccentricity is characterized by a displacement of the rotation axis of the rotor with regard to the geometric centre of the stator. Since the rotor is not centered within the stator bore, the field distribution in the airgap is no longer symmetrical. Dynamic eccentricity occurs when the rotation axis of the rotor does not coincide with its geometric centre. In practice, static and dynamic eccentricities tend to coexist. Under these circumstances, it is said that we are in the presence of mixed eccentricity [3], [9]-[13], [15].

In case a motor develops static eccentricity, the field distribution in the airgap is no longer symmetrical. As a result of that, the eccentricity creates additional motor vibrations and unbalanced magnetic pull (UMP), which can be large enough to cause a stator to rotor rub, thus resulting in serious damage to both the stator core and windings. Furthermore, eccentricity causes a non-uniform temperature distribution in the motor, hence leading to additional thermal stresses, which contribute to the appearance of other motor faults [7, 8], [12], [14].

A critical factor that shortens the motor life is heat. The insulation type used in an electric motor depends on the temperature at which motor will operate. The relationship between temperature and its effects on the life of the motor's insulation system has been studied for many years. *Montsinger* has introduced the concept of the 10º C rule according to which the life of the insulation system is halved for each additional 10º C in the temperature at which it is exposed [3]-[6]. Accordingly to IEC standards, the insulating materials used in electric motors can be classified into four thermal classes, which are presented in Table 1.

Fig 1 shows the life of the insulation system versus the temperature rise [16]. For instance from Fig.1, for a class F insulation material, an increase of 10ºC (from 160º-170º) in temperature will lead to a reduction of about 10000 h in the insulation lifetime.

The research results presented in this paper aim to investigate the temperature distribution in a 4kW, class F induction motor with static eccentricity. This study is developed through a thermal model of the motor, based on a finite element analysis.

Table 1. Thermal classes of insulating materials (adapted from standards IEC 60085, IEC 60034-1).

Temperature class	Hot spot allowance (Cº)
A	105
B	130
F	155
H	180

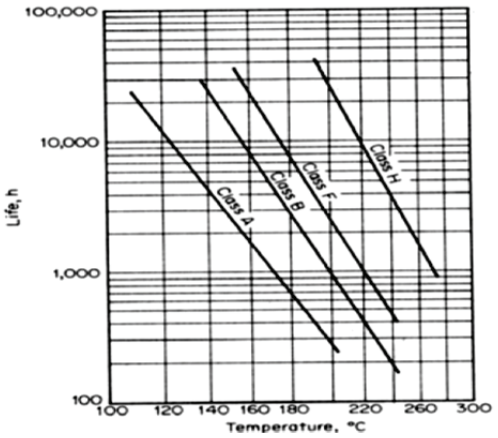

Fig. 1. Insulation life versus temperature rise.

2D Finite-Element Model

In order to analyze the motor temperature distribution under the presence of static eccentricity, several simulation tests were performed using a finite element model (FEM) developed for this purpose.

The test motor used in the simulations is a totally enclosed fan cooled (*TEFC*) three-phase squirrel-cage induction motor of 4 kW, 380 V, 50 Hz, 9.2 A, 1436.25 rpm, 26.6 N.m, cos (Φ)=0.8, with an airgap of 0.28 mm. The stator windings are star-connected.

Initially, a steady-state magnetic application, coupled with the electric circuit shown in Fig. 3, was taken into consideration, to calculate the nominal motor characteristics. A correct knowledge of the values of all elements of that circuit is essential to obtain accurate results. The mobile part of the motor is shown in the electric circuit with the bars made of conductive material (aluminum), represented by *M1, M2…M28*. On the other hand, *L4, L5…L31* represent the leakage inductance of the bars, which is calculated using (1)-(2). Moreover, to model the squirrel cage it is necessary to include the end-rings that short-circuit the rotor bars. Each segment of the end-

rings is modeled through a resistance (*R29…R84*) series-connected with a leakage inductance (*L32…L87*), whose values are calculated using (3)-(15) and (16)-(17), respectively. The stator circuits are fed with a balanced voltage supply system consisting in three sinusoidal voltage sources, V_R, V_S and V_T with a rms value of 220 V. Each phase has two stranded coils (*B1, B2, B3, B4, B5, and B6*) in order to represent the going and back side of each coil. The resistances of those stranded coils are calculated by (23) and (24), while the end winding region is represented by *L1, L2* and *L3* and calculated using (18)-(22).

Fig. 2 shows the geometrical mesh model of the induction motor and Table 2 contains the solver information of FEM. Simulations were performed with a simulated environment temperature of 20ºC.

(1) $$\lambda_r = \frac{h_r}{3*b_1}\left(1-\frac{\pi*b_1^2}{8*S_b}\right)^2 + 0.66 - \frac{h_{0r}}{2*b_1} + 0.3 + 1.12*h_{0r}*\frac{10^3}{l_b^2}$$

(2) $$L_b = \mu_0 * l_b * \lambda_r$$

(3) $$R_{er} = \frac{\rho_{Al}*\pi*p(D_r-D_i)}{e*h} * \frac{(D_r^2)^p+(D_i^2)^p}{(D_r^2)^p-(D_i^2)^p}$$

(4) $$\delta = \sqrt{\frac{4\pi^2*f_1}{\rho_{Al}*10^7}}$$

(5) $$\xi = h_b * \delta$$

(6) $$K_x = \xi * \frac{\sinh(2\xi)+\sin(2\xi)}{\cosh(2\xi)-\cos(2\xi)}$$

(7) $$h_x = h_{beq} - \frac{D_{eb}-D_e}{2} = h_{beq} \quad , D_{eb} = D_e$$

(8) $$h_{eq} = \frac{\rho_{Al}*\pi*D_e}{R_{er}*e+\pi*\rho_{Al}}$$

(9) $$X = \frac{h_{eq}}{h_x}$$

(10) $$k = \begin{cases} 0.01X^2 - 0.08X + 1.07 & if\ X < 2.36 \\ -0.017X + 0.977 & otherwise \end{cases}$$

(11) $$h_{beq} = \frac{h_b}{K_x}$$

(12) $$e_{eq} = \frac{e*k}{K_x}$$

(13) $$D_{req} = D_{eb} - h_{beq} - h_{or} * 2$$

(14) $$D_{ieq} = D_{eb} - h_{eq} * 2$$

(15) $$R_{ers} = \frac{1}{N_r}\frac{\rho_{Al}*\pi*p(D_{req}-D_{ieq})}{e_{eq}*h_{eq}} * \frac{(D_{req}^2)^p+(D_{ieq}^2)^p}{(D_{req}^2)^p-(D_{ieq}^2)^p}$$

(16) $$\lambda_i = \frac{2.3*D_{ii}}{4*N_r*L*(\sin\frac{\pi*p}{N_r})^2} * \log\left(\frac{4.7*D_{ii}}{(e+2*h)}\right)$$

(17) $$L_{ei} = 4\pi * 10^{-7} * L_i * \lambda_i$$

(18) $$L_{ew} = \frac{\pi}{2*p}\left(D_{S\_int} + 2 * h_{ss}\right) + 2 * h_{ss}$$

(19) $$L_{ap} = \frac{\pi}{2*p} * \left(D_{S\_int} + h_{ss}\right)$$

(20) $$\gamma = 0.67 * L_{ew} - 0.43 * L_{ap}$$

(21) $$L_{cb} = \frac{\mu_0}{18*p} * \frac{(N_{tsp}N_{sp})^2}{N_c} *$$

(22) $$L_t = 2 * L_{cb}$$

(23) $$R_{cu} = \rho_{cu} * \frac{L}{S_{cu}}$$

(24) $$R_{group} = N_{spp} * R_{cu}$$

where: λ_r – rotor permeance, R_{er} – end ring resistance, R_{ers} – end-ring segment resistance, ρ_{Al} – aluminum resistivity, ρ_{Cu}– copper resistivity, S_{cu} – cross-section area of the conductor, p – number of pole pairs, δ – skin effect, f_1– current stator frequency, ξ – translates the variation of the useful height of the bar, K_x – skin effect coefficient in the thickness of a bar, k – coefficient: depends on the contact surface between the bar and end-ring, λ_i – permeance between two adjacent bars, N_r – number of rotor bars, L_{ei} – leakage inductance between two adjacent bars, γ – end winding permeance, L_{cb} – end winding inductance, μ_0 – permeability of vacuum, N_{tsp} – number of turns per slot per phase, N_{sp} – number of stator slots, N_c – number of coils in parallel per phase, R_{cu} – resistance of the copper windings, R_{group} – resistance of group, N_{spp} – number of coils in series per phase, and h_r, b_1, S_b, h_{0r}, l_b, D_r, D_i, D_{ii}, e, e_{eq}, h, h_b, h_{beq}, h_x, D_{eb}, D_e, h_{eq}, D_{reg}, X, D_{ieq}, L_i, L_{ew}, D_{s_int}, h_{ss}, L_{ap} are geometric variables.

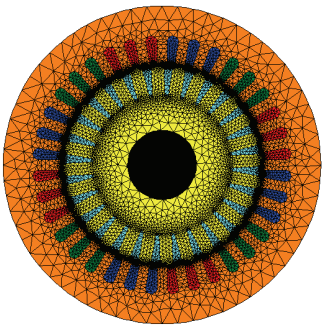

Fig. 2. Geometrical model and illustration of the finite element mesh.

Table 2. Solver information

Eccentricity level	Matrix (solver):number of lines	Excellent quality elements (%)
0	110104	94.95
3/6	117301	91.12
5/6	115384	88.48

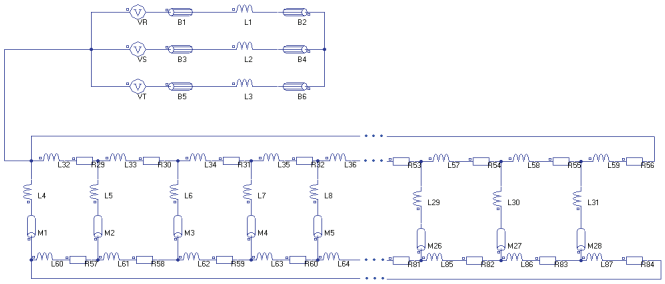

Fig. 3. Electric circuit coupled to the geometrical model.

Finally, the procedure followed to introduce static eccentricity in the model is illustrated in Fig. 4. The *dx* variable represents the eccentricity deviation, along the *x*-axis, with regard to the normal position.

Simulation Results

The simulation tests were performed for a healthy and eccentric motor, with a load torque of 26.6 N.m. Moreover, different levels of eccentricity were simulated, namely 1/6, 2/6, 3/6, 4/6 and 5/6. Due to the lack of space, this paper only presents results for the case of the motor running in healthy conditions as well as when it has an eccentricity level of 3/6 and 5/6, as summarized in Table 3.

Fig. 5 shows the temperature distribution in the stator of the motor when it is in healthy conditions. As it can be observed, the stator temperature varies in the radial direction and has a symmetric distribution with regard to the center of the rotor, meaning that the points located along a

circular radius path centered at point (0,0) have an identical temperature.

Table 3. Simulated eccentricity levels.

Eccentricity	% Eccentricity	*dx* (mm)
0	0	0
3/6	50.00	0.140
5/6	83.33	0.233

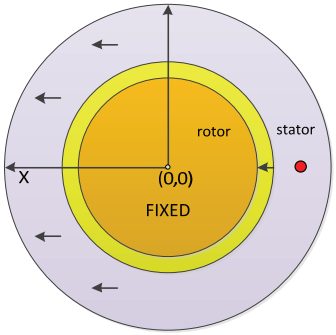

Fig.4. Introduction of eccentricity in the model.

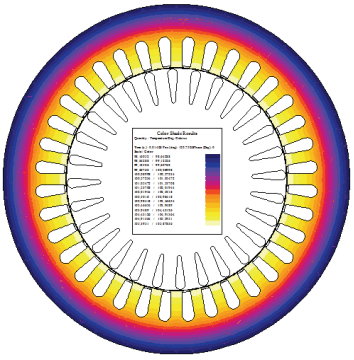

Fig.5. Healthy machine temperature distribution.

It can be observed that when the motor has eccentricity, the temperature distribution is no longer symmetrical in relation to point (0,0). There is a 4.5 ºC variation along the selected path. Note that Fig. 7 b) is rotated 90 degrees clockwise compared to Fig 4.

Finding the highest winding temperature spots is crucial to insulation (and machine) working life. The highest temperature spots in the stator are shown in Table 4. By comparing the case of the healthy motor with the situation of 5/6 eccentricity, it is observed an increase of 6.61 ºC in temperature.

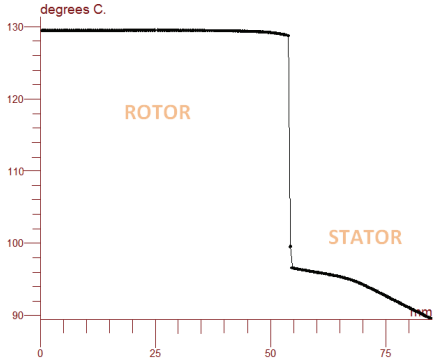

Fig.6. Radial temperature distribution.

Fig.6 depicts the radial temperature variation. It is important to notice the higher rotor temperature compared to the stator. Moreover the rotor temperature gradient is much smaller. The rotor is one of the major heat sources in the motor. The temperature distribution in the motor, in the presence of eccentricity, is shown in Fig. 7.

Fig. 7 a) shows the temperature variation of the points located along a circular path centered at point (0,0). Fig. 7 b) shows the temperature distribution in the stator with an eccentricity level of 3/6.

To complement the results presented so forth, Fig. 8 shows the temperature evolution at a point in the stator (red round marker in Fig. 4 at |X|=72 mm and |Y|=0 mm), for the non-eccentric motor (represented by the blue line) and for the motor with two different levels of static eccentricity: 3/6 (represented by the red line) and 5/6 (represented by the green line). As it can be seen, for the same point, three different temperature curves are obtained, hence supporting the conclusion that eccentricity increases the maximum motor temperature.

On the other hand, for the eccentric motor, the field distribution in the airgap is no longer symmetrical. As a consequence of that, it gives rise to an UMP as mentioned before.

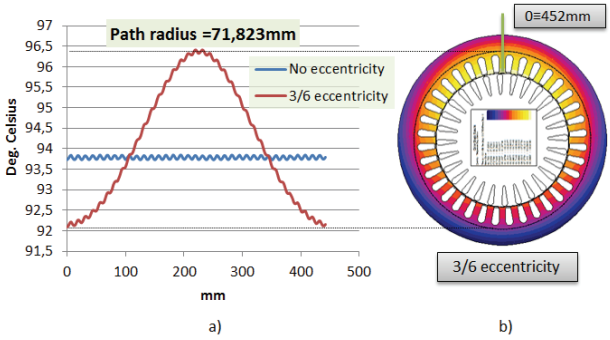

Fig.7. Temperature distribution in the eccentric motor, and comparison with the normal situation.

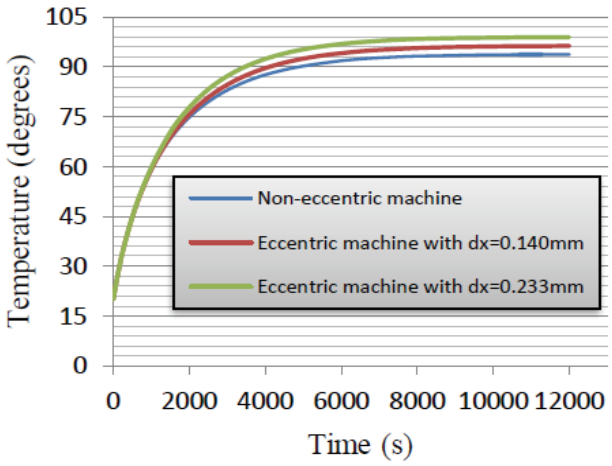

Fig.8. Temperature evolution for a given location.

Table 4. Highest temperature spot in the stator.

Eccentricity level	*Highest temperature spot in the stator (degree C°)*
0	96.68
3/6	99.87
5/6	103.29

Figs. 9 and 10 show the flux density magnitude and radial airgap length along a circular radius path in the airgap, plotted against an angular position measured with regard to the stator, for the non-eccentric and eccentric motor with 5/6 of eccentricity, respectively. As it can be

seen from Fig. 10, when the airgap length decreases (blue line), the flux density magnitude increases, in contrast with what is shown in Fig 9.

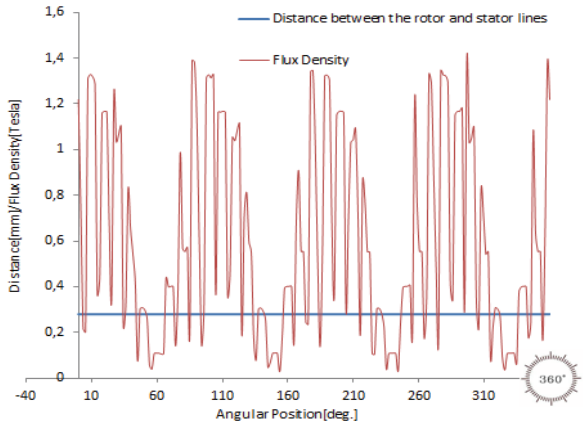

Fig.9. Airgap flux density versus versus angular position (healthy motor).

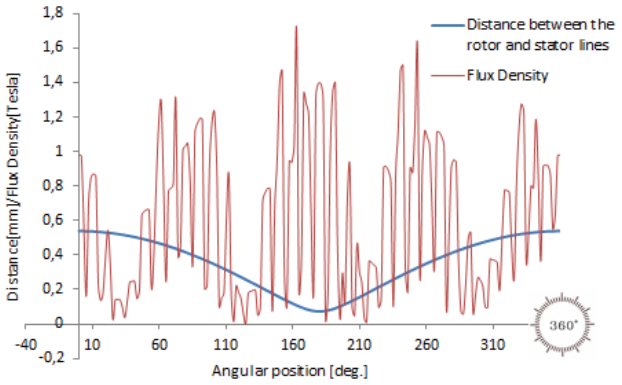

Fig.10. Airgap flux density and radial airgap length versus angular position (5/6 eccentricity level).

Conclusion

The temperature rise inside the motor can affect several motor components such as the stator windings. These simulation results shown in this paper have demonstrated that motor faults such as eccentricity cause a non-uniform distribution of temperature in the motor, as well as an increase in the highest stator temperature. Since the motor lifespan is directly related to its working temperature, the eccentricity, if present for long periods of time, can shorten the lifetime of the insulation system of the windings, which may eventually lead to a failure in this motor component.

Further studies are to be conducted in order to show the influence of other types of eccentricity in the motor temperature.

Acknowledgement

The authors wish to acknowledge the financial support of the Fundação para a Ciência e a Tecnologia (FCT) under project number PTDC/EEA-EEL/100156/2008.

REFERENCES

[1] Barbour, A.; Thomson, W.T.; "Finite element study of rotor slot designs with respect to current monitoring for detecting static airgap eccentricity in squirrel-cage induction motors" Industry Applications Conference, 1997. Thirty-Second IAS Annual Meeting, IAS '97., Conference Record of the 1997 IEEE , vol.1, no., pp.112-119 vol.1, 5-9 Oct 1997.

[2] M. B. Bannae Sharifian, Jawad Faiz, and Bashir Mahdi Ebrahimi "Analysis of Induction Motor Static Eccentricity using Time Stepping Finite Element ", International Conference on Electrical Machines, ICEM 2006, Conf. Publ. No. 289, September, 2-5, 2006.

[3] Drif, M'hamed; Cardoso, A.J. Marques, "Airgap Eccentricity Fault Diagnosis, in Three-Phase Induction Motors, by the Instantaneous Power Signature Analysis," The 3rd IET International Conference on Power Electronics, Machines and Drives, 2006, vol., no., pp.349-353, Mar. 2006.

[4] Don-Ha Hwang; Ki-Chang Lee; Joo-Hoon Lee; Dong-Sik Kang; Jin-Hee Lee; Kyeong-Ho Choi; , "Analysis of a three phase induction motor under eccentricity condition," Industrial Electronics Society, 2005. IECON 2005. 31st Annual Conference of IEEE , vol., no., pp. 5 pp., 6-10 Nov. 2005.

[5] Marques Cardoso, A.J.; Saraiva, E.S.; Sousa Mateus, M. L.; Ramalho, A.L.; "On-line detection of airgap eccentricity in 3-phase induction motors, by Park's Vector approach," Fifth International Conference on Electrical Machines and Drives, 1991. (Conf. Publ. No. 341), vol., no., pp.61-66, 11-13 Sep 1991.

[6] Mendes, A.M.S.; Lopez-Fernandez, X.M.; Marques Cardoso, A.J.; "Thermal Performance of a Three-Phase Induction Motor Under Fault Tolerant Operating Strategies," IEEE Transactions on Power Electronics, vol.23, no.3, pp.1537-1544, May 2008.

[7] A. C. Smith and D. G. Dorell, "Calculation and measurement of unbalanced magnetic pull in cage induction motors with eccentric rotors. Part 2: Experimental investigation," IEE Proc. Electr. Power Appl., vol.143, no. 3, pp. 202–210, 1996.

[8] R. Fiser, "Application of a finite element method to predict damaged induction motor performance," IEEE Trans. Magn., vol. 37, no. 5, pp. 3635–3639, Sep. 2001.

[9] S. Nandi, R. M. Bharadwaj, and H. A. Toliyat, "Performance analysis of a three-phase induction motor under mixed eccentricity condition," IEEE Trans. Energy Convers., vol. 17, no. 3, pp. 392–399, Sep. 2002.

[10] S. Nandi, S. Ahmed, and H. A. Toliyat, "Detection of rotor slot and other eccentricity related harmonics in a three phase induction motor with different rotor cages," IEEE Trans. Energy Convers., vol. 16, no. 3, pp. 253–260, Sep. 2001.

[11] Grieger, J.; Supangat, R.; Ertugrul, N.; Soong, W.L.; "Induction Motor Static Eccentricity Severity Estimation Using Evidence Theory," IEEE International Electric Machines & Drives Conference, 2007. IEMDC '07, vol.1, no., pp.190-195, 3-5 May 2007.

[12] Vitek, O.; Janda, M.; Hajek, V.; "Effects of eccentricity on external magnetic field of induction machine," MELECON 2010 - 2010 15th IEEE Mediterranean Electrotechnical Conference, vol., no., pp.939-943, 26-28 April2010.

[13] Xiaodong Li; Nandi, S.; "Analysis of a 3-phase induction machine with inclined static eccentricity," Electric Machines and Drives, 2005 IEEE International Conference on , vol., no., pp.1606-1613, 15-15 May 2005.

[14] Nandi, S.; Ilamparithi, T.C.; Sang Bin Lee; Doosoo Hyun; "Detection of Eccentricity Faults in Induction Machines Based on Nameplate Parameters," IEEE Transactions on Industrial Electronics, vol.58, no.5, pp.1673-1683, May2011.

[15] Faiz, J.; Ebrahimi, B.M.; Akin, B.; Toliyat, H.A.; "Finite-Element Transient Analysis of Induction Motors Under Mixed Eccentricity Fault," IEEE Transactions on Magnetics, vol.44, no.1, pp.66-74, Jan. 2008.

[16] The Induction Machines Design Handbook, 2nd Edition (Boldea, I. and Nasar, S.A.).

***Authors**: Bruno Baptista, University of Coimbra/Instituto de Telecomunicações, E-mail: brunobapt@gmail.com; André Mendes, University of Coimbra/Instituto de Telecomunicações, E-mail: amsmendes@ieee.org; Sérgio Cruz, University of Coimbra/Instituto de Telecomunicações, E-mail: smacruz@ieee.org; António Cardoso, University of Coimbra/Instituto de Telecomunicações, E-mail: ajmcardoso@ieee.org*